Nanoscale

RSC Publishing

COMMUNICATION

View Article Online
View Journal | View Issue

Phase transformation and thermoelectric properties of bismuth-telluride nanowires†

Cite this: *Nanoscale*, 2013, **5**, 4669

Received 19th February 2013
Accepted 1st April 2013

DOI: 10.1039/c3nr00876b

www.rsc.org/nanoscale

Cheng-Lun Hsin,‡*[a] Matthew Wingert,‡[b] Chun-Wei Huang,[c] Hua Guo,[d] Ten-Jen Shih,[a] Joonki Suh,[d] Kevin Wang,[d] Junqiao Wu,[de] Wen-Wei Wu[c] and Renkun Chen*[b]

Thermoelectric materials have attracted much attention due to the current interest in energy conversion and recent advancements in nano-engineering. A simple approach to synthesize BiTe and Bi_2Te_3 micro/nanowires was developed by combining solution chemistry reactions and catalyst-free vapor–solid growth. A pathway to transform the as-grown BiTe nanostructures into Bi_2Te_3 can be identified through the Bi–Te phase diagram. Structural characterization of these products was identified using standard microscopy practices. Meanwhile, thermoelectric properties of individual Bi–Te compound micro/nanowires were determined by the suspended microdevice technique. This approach provides an applicable route to synthesize advanced high performance thermoelectric materials in quantities and can be used for a wide range of low-dimensional structures.

Technologies for converting waste heat into useful electricity have become an important research topic in recent years.[1–5] For this purpose, thermoelectric materials, which can generate electricity while under a temperature gradient, have attracted much attention following advances in nano-engineering materials. For practical applications, which may have different working temperature requirements, the development of materials with high thermoelectric efficiency that can be mass produced cheaply is paramount. Besides, the energy cost for the production and high-end facility needed for highly efficient superlattice/quantum nanostructures needs to meet commercial requirements. Therefore, synthesis and material processing play essential roles in practical applications. Nanomaterials are expected to enhance the thermoelectric figure-of-merit due to quantum confinement effects and increased surface phonon scattering.[6–8] Among the best thermoelectric materials, Bi–Te compounds, including Bi_2Te_3 and related alloys,[9,10] are frequently used in commercial solid state Peltier coolers and low temperature thermal couples, and show promise for thermal energy scavenging.[11] Conventional fabrication processes for Bi_2Te_3 and related ternary compound nanowires, such as electrodeposition, are complex and require electrochemical workstations. In this study, we developed a simple and fast approach to grow BiTe nanostructures using chemically synthesized BiTe nanoparticles as precursors. The as-synthesized BiTe nanostructures were transformed into Bi_2Te_3 by thermal annealing in the presence of Te vapor. The temperature dependent thermoelectric properties of BiTe and the transformed Bi_2Te_3 were investigated, exhibiting drastically enhanced figure-of-merit after the transformation. These results prove that this method is a simple, feasible route to produce high quality thermoelectric nanomaterials in quantities.

All chemicals were obtained from Sigma Aldrich and used without further purification. Bismuth telluride (BiTe) nanoparticles were synthesized by mixing 0.2 mmol $BiCl_3$ (99.99%) in 1 ml nitric acid and 0.3 mmol H_6TeO_6 (99.99%) in 2 ml deionized water, followed by the addition of 1 mmol thioglycolic acid (98%) for the formation of the mixed complex at room temperature. Then the solution temperature was raised to 90 °C and 1 ml hydrazine monohydrate (98%) was added for the reduction of the BiTe nanoparticles.[12] The as-synthesized nanoparticles were filtered and washed with excess acetone, then collected and drop-cast with acetone onto silicon (100) wafers which had been ultrasonically cleaned in an acetone solution for 30 min to remove organic residues, rinsed with deionized water and subsequently cleaned through a standard RCA process and dilute HF dip for 10 s.[13,14] Substrates with

[a]*Department of Electrical Engineering, National Central University, Taoyuan 32001, Taiwan. E-mail: clhsin@ee.ncu.edu.tw*

[b]*Department of Mechanical and Aerospace Engineering, University of California, La Jolla, San Diego, California 92093, USA. E-mail: rkchen@ucsd.edu*

[c]*Department of Materials Science and Engineering, National Chiao Tung University, Hsinchu 300, Taiwan*

[d]*Department of Materials Science and Engineering, University of California, Berkeley, California 94720, USA*

[e]*Materials Sciences Division, Lawrence Berkeley National Laboratory, Berkeley, CA 94720, USA*

† Electronic supplementary information (ESI) available. See DOI: 10.1039/c3nr00876b

‡ These authors contributed equally to this work.

nanoparticles were placed face-to-face in a furnace and annealed at 600 °C in a vacuum (10^{-3} torr) for 30 min. Before annealing, the furnace was purged with Ar for 20 min and pumped to low pressure to remove oxygen. Acetone will vaporize easily under atmosphere conditions and furnace purification in a vacuum. BiTe nanostructures were grown during annealing on the substrates. BiTe nanowires were then dried, transferred to a new Si substrate and loaded into a furnace, purged with Ar, and annealed at 400 °C in vacuum (10^{-3} torr) for 3 h. During the annealing process, pure Te powder (99.8%) was placed next to the samples, serving as a Te source for transforming BiTe into Bi_2Te_3.

Thermoelectric properties were measured using suspended micro-device heaters over a temperature range of 300–500 K. Pt resistance thermometer coils patterned onto the suspended membranes allow for heating and temperature sensing, where one coil acts as a heater to create a temperature differential across the micro/nanowire and both coils simultaneously act as thermometers to measure the temperature rise of each suspended membrane. Such devices have previously been used for single nanowire thermal conductivity measurements.[3,15–17] Four electrodes, two bonded to each end of the micro/nanowire with Pt by focused ion beam (FIB), allow for 4-point *I–V* resistivity measurements as well as Seebeck voltage measurements while heating the micro/nanowires (see Fig. 3). The details of the Seebeck and resistivity measurements are described in the ESI.† Measurements were performed in a vacuum chamber evacuated to ~10^{-5} torr to reduce conduction and convection heat transfer due to residual air molecules to negligible quantities. The micro/nanowires are large enough that all non-negligible heat transfer occurs by conduction through the wire itself.

A JEOL 6500 field-emission scanning electron microscope (SEM) and a 2100F transmission electron microscope (TEM) equipped with an energy dispersion spectrometer (EDS) were used to image microstructures and determine chemical composition. Fast Fourier transform (FFT) was used to reduce noise in the high resolution TEM image and analyze the diffraction pattern.

Fig. 1(a) shows an SEM image of an as-grown BiTe micro/nanowire with length greater than 10 μm. Due to the absence of a catalyst, the growth of BiTe nanostructures is attributed to the vapor–solid mechanism, which results in a diverse set of morphologies, including nanowires, nanobelts, and microwires. Fig. 1(b) depicts the EDS spectrum of the samples, with the inset listing composition, indicating a deficiency of Te in the BiTe nanowires. A TEM image of a BiTe nanowire is shown in Fig. 1(c) along with the EDS line scan. The TEM image also reveals the surface roughness of the nanowires. Lattice planes are clearly evident in the high-resolution TEM image of the nanowire, shown in Fig. 1(d). The FFT pattern in the inset of Fig. 1(d) from the high-resolution TEM (HRTEM) image confirms that the BiTe nanowire has a $P\bar{3}m1$ hexagonal structure.

Fig. 2(a) and (b) show optical images of the as-transferred BiTe micro/nanowires and their as-transformed Bi_2Te_3 counterparts, respectively. During the annealing process in a Te rich atmosphere and at high temperature, transformation of BiTe to Bi_2Te_3 occurred in the Te-supersaturated region, which allowed

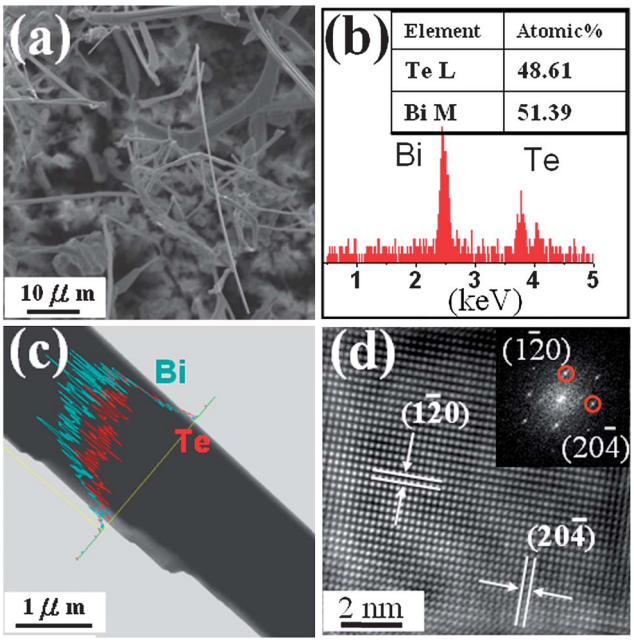

Fig. 1 (a) SEM image of the as-grown BiTe nanostructures on the Si substrate, (b) EDS spectrum of the BiTe nanostructures. The inset is the atomic percentage of the elements, (c) TEM image of the BiTe nanobelt, and (d) the high resolution TEM image of the BiTe nanobelt. The inset is the corresponding FFT electron diffraction pattern.

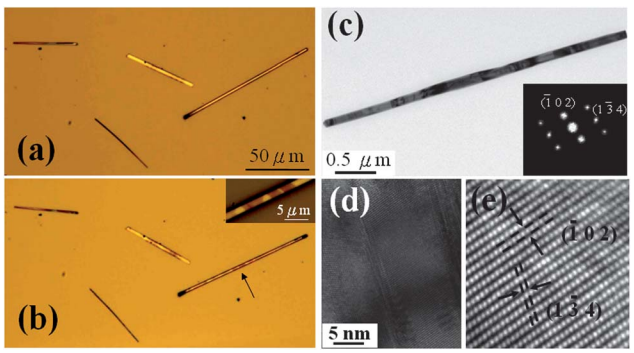

Fig. 2 (a) Optical image of the BiTe nanostructures and (b) the corresponding optical image of the Bi_2Te_3 nanostructures. The inset is the high magnification image highlighted with an arrow in (b), (c) TEM image of the as-transformed Bi_2Te_3 nanowire. The inset is the FFT diffraction pattern, (d) high magnification TEM image of the Bi_2Te_3 nanowire at the twin boundary, and (e) the HRTEM image of the nanowire.

for the incorporation of Te into BiTe. Based on the phase diagram of Bi–Te,[18] BiTe will react with Te in this state and form Bi_2Te_3. This transformation may not occur at the same rate along an individual micro/nanowire or may have multiple nucleation sites, possibly resulting in polycrystalline Bi_2Te_3. The optical contrast of Bi_2Te_3 products in Fig. 2(b) shows evidence of the existence of multiple grain boundaries. The inset of Fig. 2(b) depicts the contrast of the grain boundary of the nanowire highlighted with an arrow. For comparison, TEM images of the nanowire were taken after transformation, shown in Fig. 2(c). The polycrystalline structure of the nanowire is

evident and the FFT diffraction pattern in the inset was taken from the HRTEM image in Fig. 2(e). The grain/twin boundary is highlighted in Fig. 2(d), demonstrating the defects of two adjacent grains, which are the result of an inhomogeneous phase transformation.

Fig. 3 shows the SEM image of a device used to characterize the thermoelectric properties of the nanowires. The device consists of two suspended silicon nitride membranes with serpentine heating and sensing coils and four Pt electrodes. Nanowires were transferred to bridge the pads. During the measurement, the temperature of one pad was raised, with heat conducting through the nanowire resulting in a temperature difference between the two pads. Pt contacts were deposited using a FIB to secure the transferred micro/nanowire to the electrodes. Excess length of the micro/nanowire was cut to eliminate electrical shorting.

Temperature-dependent thermoelectric properties of the as-grown BiTe and transformed Bi_2Te_3 nanowires are summarized in Fig. 4. The uncertainties in the measured k, ρ, S, and ZT are 15–18%, 6–8%, ~20% and 30–33%, respectively (ESI†). The thermal conductivities of BiTe and Bi_2Te_3 nanowires (Fig. 4(a)) are about 4.5 and 1.2 W m^{-1} K^{-1} at 300 K, respectively. The BiTe nanowire has a higher electrical conductivity and hence a larger electronic thermal conductivity. However, this alone would not explain the significantly higher thermal conductivity (k_e in the BiTe nanowire is only 0.7 W m^{-1} K^{-1}). It was also recognized that the total thermal conductivity of the BiTe nanowire is significantly higher than that of the $Bi_{0.515}Te_{0.485}$ single crystal (1.83 W m^{-1} K^{-1} at 300 K).[19] Therefore, the higher thermal conductivity in the BiTe nanowire must be the result of a larger bipolar contribution and higher lattice thermal conductivity, which are difficult to quantify without a complete modeling of carrier and phonon transport.

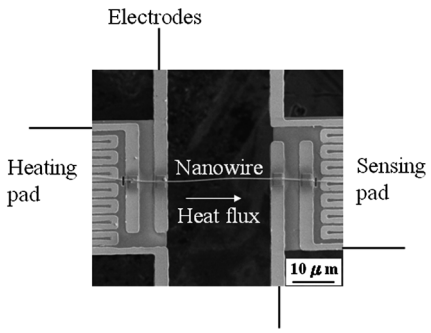

Fig. 3 The SEM image of a micro-fabricated device used for single nanowire thermoelectric property measurements.

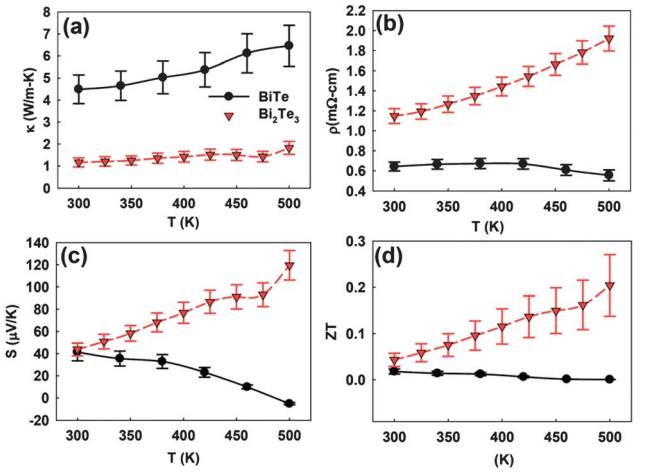

Fig. 4 Temperature-dependent thermoelectric properties of BiTe (black circles) and Bi_2Te_3 (red down triangles). (a) Thermal conductivity, (b) electrical resistivity, (c) Seebeck coefficient, and (d) ZT.

The thermal conductivity of Bi_2Te_3 is much lower than that of bulk single crystal Bi_2Te_3 (1.73 W m^{-1} K^{-1}),[19] showing the effectiveness of phonon scattering by nanowire surfaces, grain boundaries and defects, which is advantageous for thermoelectrics. However, the thermal conductivity of our Bi_2Te_3 nanowires is higher than that of the nanostructured bulk counterpart,[20] presumably due to the larger grain size in our samples.

The total thermal conductivity of both BiTe and Bi_2Te_3 nanowires increases gradually with temperature, and the trend is more pronounced for the BiTe nanowire. The temperature dependence can be attributed to the onset of bi-polar diffusion at higher temperature. The more pronounced trend for the BiTe nanowire is also consistent with the rapid decreasing Seebeck coefficient with temperature. Similarly, increasing temperature dependence for total thermal conductivity has also been observed in $Bi_{1.5}Sb_{0.5}Te_3$ nano-composites.[21–23]

The electrical resistivity of the as-grown BiTe micro/nanowires is as low as 0.6 mΩ cm, while that of Bi_2Te_3 is ~1.1 mΩ cm (Fig. 4(b)). From the EDS in Fig. 1(b), BiTe is non-stoichiometric with excess Bi. Grain boundaries in the transformed Bi_2Te_3 micro/nanowires may be a major source of electron scattering, resulting in decreased electron mobility. The electrical resistivity of BiTe and Bi_2Te_3 shows opposing temperature dependences: BiTe exhibits semiconducting behavior (resistivity decreases with temperature) while Bi_2Te_3 exhibits metallic behavior (resistivity increases with temperature). This reveals that Bi_2Te_3 must have a degenerate free electron density due to extrinsic and unintentional dopants (such as native defects and impurities from the Te powder), and its higher resistivity could be caused by lower mobility.

The opposing temperature dependence of electrical resistivity in BiTe and Bi_2Te_3 correlates well with the behavior of their thermopower (Seebeck coefficient). The Seebeck coefficient is positive for both BiTe and Bi_2Te_3 (Fig. 4(c)), except for BiTe at 500 K where it approaches zero. Two conclusions can be drawn from these results: (1) holes are responsible for electrical transport, and both materials are p-type. This suggests that the materials are Bi-rich.[24] (2) Intrinsic carriers thermally activated across the bandgap of BiTe also play an important role to such a degree that at high temperatures (>500 K) its Seebeck coefficient approaches −4 μV K^{-1} due to bi-polar conduction. On the other hand, the linearly increasing Seebeck coefficient with respect to the temperature in Bi_2Te_3 is consistent with the behavior expected from a metallically doped material.[25]

The thermoelectric figure-of-merit is given by $ZT = S^2T/\rho\kappa$, where S, ρ, T, and κ are the Seebeck coefficient, electrical resistivity, absolute temperature, and thermal conductivity,

respectively, and are shown as functions of T in Fig. 4(d). The ZT of the Bi_2Te_3 nanowires increases with temperature as opposed to that of BiTe, which decreases. At high temperatures, the ZT of Bi_2Te_3 is much greater (by >500 times) than that of BiTe prior to transformation. In comparison to previous reports of electrodeposited Bi_2Te_3 nanowires,[26] ZT is of the same magnitude but lower than that of its bulk counterpart due to the high electrical resistivity, which is three times higher than that of the bulk property.[20] In addition, the higher resistivity of our result suggested processing control to suppress the unexpected impurity and electron-defect scattering. ZT could also be improved through further optimization of material processing and the resultant structure. For example, the carrier and heat conduction along the a-plane is 4 and 2 times higher than that of the c-axis direction, respectively, indicating that crystallographic orientation is one way to improve ZT.[27] Meanwhile, alloying with Sb and Se is another option to improve ZT by way of modifying the phonon scattering and electronic density of states.[6]

In summary, BiTe and Bi_2Te_3 micro/nanowires were synthesized using a simple and low cost chemical reaction and thermal annealing process. The structure and composition were investigated using SEM, TEM, and micro-Raman. The BiTe micro/nanowires were successfully transformed into Bi_2Te_3 by thermal annealing in the presence of Te vapor. Temperature dependent thermoelectric properties (thermal conductivity, resistivity, Seebeck coefficient) were measured and the figure-of-merit, ZT, was found to increase after the transformation of BiTe to Bi_2Te_3, reaching $\sim$0.2 at 500 K. The methodology presented here is applicable for synthesis of Bi–Te nanostructures and could possibly be extended to other bismuth—group VI compound alloys due to similarities in the binary phase diagrams of Bi—O, S, and Se for the future design of thermoelectric materials.

Acknowledgements

The authors acknowledge the support from Taiwan National Science Council (NSC) Grants 101-2218-E-008-014-MY2, 101-3113-P-008-008-, 100-2628-E-009-023-MY3, National Science Foundation (NSF) under Grant no. CBET-0932905, Department of Energy BES-LBL thermoelectrics program (DE-AC02-05-CH11231) and National Center for Electron Microscopy, Lawrence Berkeley Lab (DE-AC02-05CH11231).

References

1 A. I. Boukai, Y. Bunimovich, J. Tahir-Kheli, J. K. Yu, W. A. Goddard and J. R. Heath, *Nature*, 2008, **451**, 168–171.
2 O. Bubnova, Z. U. Khan, A. Malti, S. Braun, M. Fahlman, M. Berggren and X. Crispin, *Nat. Mater.*, 2011, **10**, 429–433.
3 A. I. Hochbaum, R. K. Chen, R. D. Delgado, W. J. Liang, E. C. Garnett, M. Najarian, A. Majumdar and P. D. Yang, *Nature*, 2008, **451**, 163–U165.
4 A. J. Minnich, M. S. Dresselhaus, Z. F. Ren and G. Chen, *Energy Environ. Sci.*, 2009, **2**, 466–479.
5 H. Z. Zhao, M. Pokheral, G. H. Zhu, S. Chen, K. Lukas, Q. Jie, C. Opeil, G. Chen and Z. F. Ren, *Appl. Phys. Lett.*, 2011, **99**, 163101.
6 M. S. Dresselhaus, G. Chen, M. Y. Tang, R. G. Yang, H. Lee, D. Z. Wang, Z. F. Ren, J. P. Fleurial and P. Gogna, *Adv. Mater.*, 2007, **19**, 1043–1053.
7 A. Li Bassi, A. Bailini, C. S. Casari, F. Donati, A. Mantegazza, M. Passoni, V. Russo and C. E. Bottani, *J. Appl. Phys.*, 2009, **105**, 124307.
8 J. R. Szczech, J. M. Higgins and S. Jin, *J. Mater. Chem.*, 2011, **21**, 4037–4055.
9 M. Craps, N. Gothard, R. Rao, J. Gaillard, T. Tritt and A. M. Rao, *2005 24th International Conference on Thermoelectrics (ICT) (IEEE Cat. no.05TH8854C)*, 2005, pp. 292–294.
10 X. A. Yan, B. Poudel, Y. Ma, W. S. Liu, G. Joshi, H. Wang, Y. C. Lan, D. Z. Wang, G. Chen and Z. F. Ren, *Nano Lett.*, 2010, **10**, 3373–3378.
11 D. Fukuda, S. Kimura and M. Endo, *Rev. Sci. Instrum.*, 2005, **76**, 113107.
12 A. Purkayastha, F. Lupo, S. Kim, T. Borca-Tasciuc and G. Ramanath, *Adv. Mater.*, 2006, **18**, 496–500.
13 C. L. Hsin, S. Y. Yu, C. W. Huang and W. W. Wu, *Appl. Phys. Lett.*, 2010, **97**, 181920.
14 C. L. Hsin, S. Y. Yu and W. W. Wu, *Nanotechnology*, 2010, **21**, 485602.
15 R. Chen, A. I. Hochbaum, P. Murphy, J. Moore, P. D. Yang and A. Majumdar, *Phys. Rev. Lett.*, 2008, **101**, 105501.
16 D. Y. Li, Y. Y. Wu, P. Kim, L. Shi, P. D. Yang and A. Majumdar, *Appl. Phys. Lett.*, 2003, **83**, 2934–2936.
17 L. Shi, D. Y. Li, C. H. Yu, W. Y. Jang, D. Kim, Z. Yao, P. Kim and A. Majumdar, *J. Heat Transfer*, 2003, **125**, 881–888.
18 T. Caillat, M. Carle, D. Perrin, H. Scherrer and S. Scherrer, *J. Phys. Chem. Solids*, 1992, **53**, 227–232.
19 J. P. Fleurial, L. Gailliard, R. Triboulet, H. Scherrer and S. Scherrer, *J. Phys. Chem. Solids*, 1988, **49**, 1237–1247.
20 M. Saleemi, M. S. Toprak, S. H. Li, M. Johnsson and M. Muhammed, *J. Mater. Chem.*, 2012, **22**, 725–730.
21 P. K. Nguyen, K. H. Lee, J. Moon, S. I. Kim, K. A. Ahn, L. H. Chen, S. M. Lee, R. K. Chen, S. Jin and A. E. Berkowitz, *Nanotechnology*, 2012, **23**, 415604.
22 B. Poudel, Q. Hao, Y. Ma, Y. C. Lan, A. Minnich, B. Yu, X. A. Yan, D. Z. Wang, A. Muto, D. Vashaee, X. Y. Chen, J. M. Liu, M. S. Dresselhaus, G. Chen and Z. F. Ren, *Science*, 2008, **320**, 634–638.
23 W. J. Xie, J. He, H. J. Kang, X. F. Tang, S. Zhu, M. Laver, S. Y. Wang, J. R. D. Copley, C. M. Brown, Q. J. Zhang and T. M. Tritt, *Nano Lett.*, 2010, **10**, 3283–3289.
24 M. Takahashi, M. Kojima, S. Sato, N. Ohnisi, A. Nishiwaki, K. Wakita, T. Miyuki, S. Ikeda and Y. Muramatsu, *J. Appl. Phys.*, 2004, **96**, 5582–5587.
25 A. X. Levander, T. Tong, K. M. Yu, J. Suh, D. Fu, R. Zhang, H. Lu, W. J. Schaff, O. Dubon, W. Walukiewicz, D. G. Cahill and J. Wu, *Appl. Phys. Lett.*, 2011, **98**, 012108.
26 A. Mavrokefalos, A. L. Moore, M. T. Pettes, L. Shi, W. Wang and X. G. Li, *J. Appl. Phys.*, 2009, **105**, 104318.
27 L. D. Zhao, B. P. Zhang, J. F. Li, H. L. Zhang and W. S. Liu, *Solid State Sci.*, 2008, **10**, 651–658.

